

Article

Modeling Metallic Fatigue Data Using the Birnbaum–Saunders Distribution

Zaid Sawlan ^{1,2,*} , Marco Scavino ³  and Raúl Tempone ^{4,5}

¹ Department of Mathematics, King Fahd University of Petroleum and Minerals, Dhahran 31261, Saudi Arabia

² Interdisciplinary Research Center for Refining & Advanced Chemicals, King Fahd University of Petroleum and Minerals, Dhahran 31261, Saudi Arabia

³ Instituto de Estadística (IESTA), Departamento de Métodos Cuantitativos, FCEA, Universidad de la República, Montevideo 11200, Uruguay; marco.scavino@fcea.edu.uy

⁴ Computer, Electrical and Mathematical Sciences and Engineering, King Abdullah University of Science and Technology, Thuwal 23955, Saudi Arabia; raul.tempone@kaust.edu.sa

⁵ Chair of Mathematics for Uncertainty Quantification, RWTH Aachen University, 52072 Aachen, Germany

* Correspondence: zaid.sawlan@kfupm.edu.sa

Abstract: This work employs the Birnbaum–Saunders distribution to model the fatigue-life of metallic materials under cyclic loading and compares it with the normal distribution. Fatigue-limit models are fitted to three datasets of unnotched specimens of 75S-T6 aluminum alloys and carbon laminate with different loading types. A new equivalent stress definition that accounts for the effect of the experiment type is proposed. The results show that the Birnbaum–Saunders distribution consistently outperforms the normal distribution in fitting the fatigue data and provides more accurate predictions of fatigue-life and survival probability.

Keywords: metallic fatigue data; fatigue-life prediction; fatigue-limit models; maximum likelihood methods; Birnbaum–Saunders distribution



Citation: Sawlan, Z.; Scavino, M.; Tempone, R. Modeling Metallic Fatigue Data Using the Birnbaum–Saunders Distribution. *Metals* **2024**, *14*, 508. <https://doi.org/10.3390/met14050508>

Academic Editor: Alireza Akhavan-Safar

Received: 6 March 2024

Revised: 17 April 2024

Accepted: 23 April 2024

Published: 26 April 2024



Copyright: © 2024 by the authors. Licensee MDPI, Basel, Switzerland. This article is an open access article distributed under the terms and conditions of the Creative Commons Attribution (CC BY) license (<https://creativecommons.org/licenses/by/4.0/>).

1. Introduction

Fatigue-life prediction is vital to prevent the failure of mechanical parts that are under cyclic loadings. In the field of fatigue-life assessment, two primary methodologies are commonly used: stress-life models (or S-N curves) [1–4] and linear elastic fracture mechanics (LEFM) [5–8]. The S-N curve method relies on experimental data that models stress amplitude against the number of cycles until failure. It provides a direct correlation between the cyclic stress level and the expected life of the component. This method is particularly effective for high-cycle fatigue analysis, where stresses are below the material's yield strength and failure is expected after a large number of cycles (typically over 10^4 cycles). The underlying assumption is that the material does not have initial flaws and the initiation of cracks dominates the fatigue-life. This assumption may not be valid in certain operational scenarios. For example, S-N curves are not employed in the Aircraft Structural Integrity Program (ASIP) according to USAF MIL-STD-1530D [9]. This specification highlights the importance of selecting appropriate methodologies for different operational contexts.

On the other hand, LEFM focuses on the growth of existing cracks and is governed by the principles of fracture mechanics. It relies on the concept of stress intensity factors to predict crack growth rates and the subsequent fatigue-life under cyclic loading. LEFM is most applicable to low-cycle fatigue scenarios where the stress levels are high enough to induce plasticity at the tip of the crack, and the life of the component is largely determined by the rate of crack propagation [10]. This approach is adopted by the USAF, as detailed in [9,11]. A comprehensive review of various fatigue crack types and their development in actual aerospace structures is detailed in [12]. A probabilistic extension is provided in [13] that emphasizes the role of the equivalent initial damage size (EIDS) or, equivalently,

the effective initial flaw size (EIFS) [14]. Recent works have also been developed, such as [6], which utilizes the continuum damage mechanics (CDM) theory and LEM theory to predict the total gear bending fatigue-life, and [7], which investigates the effect of crack initiation angles and plastic zones of thin-walled cylindrical shells with cracks.

The main difference between the two methodologies lies in their foundational assumptions: S-N curves assume a flaw-free material and focus on the initiation of fatigue cracks, whereas LEM assumes the presence of initial cracks and concentrates on their propagation [15].

In this current study, our focus is on high-cycle fatigue analysis with the goal of predicting the life of mechanical components made from the same material and having the same surface finish; therefore, we only consider S-N models. This choice is justified by the nature of high-cycle fatigue processes, where the material is subjected to relatively low stress levels that do not promote significant crack propagation before a very high number of cycles is reached. Moreover, considering homogeneous material and surface finish criteria, the S-N approach offers a more straightforward and practical means of predicting fatigue-life without the need for intricate crack growth analyses as is required by LEM. It is important to note that this work is an academic study based on uniform samples under controlled experimental conditions. Future work could extend these findings to more practical conditions and real-world settings.

Although there are many models to relate stress with the fatigue-life, with probabilistic models, the fatigue-life is often assumed to be a log-normal random variable [16–19] or follow a Weibull distribution [16,20,21]. In this work, we consider Birnbaum–Saunders distributions and compare the fitting of different fatigue datasets with the log-normal distribution.

Birnbaum–Saunders distributions were introduced as a two-parameter family of life distributions [22]. Several studies have used these distributions to fit fatigue datasets using the maximum likelihood [23,24] and Bayesian methods [25–27]. In addition, many variations have been proposed, such as the log-linear model for the Birnbaum–Saunders distribution [28] and the bivariate log-Birnbaum–Saunders distribution [29]. An extensive review of the Birnbaum–Saunders distribution and its generalizations is provided in [30,31].

Our goal is to study the use of Birnbaum–Saunders distributions and analyze their fitting results compared with the dominant choice of normal distributions. To this end, we use two datasets of fatigue experiments applied to specimens of 75S-T6 aluminum alloys [32,33] and a dataset of bending tests of carbon laminate [34]. Moreover, we study the effect of equivalent stress model when fatigue data includes different types of experiments.

For the S-N models, there are many possible regression models that could be considered. We focus only on the fatigue-limit type of model with constant and non-constant variance (or shape parameter). The fatigue-life variable is modeled by the log-normal distribution or Birnbaum–Saunders distribution. Equivalently, the logarithm of N is modeled by normal and sinh-normal distributions, respectively. However, we show that modeling $\log(N)$ as a Birnbaum–Saunders distribution provides better fitting results. This proposed model is unprecedented in the literature to the best of our knowledge.

The first dataset is the same data considered in [16], where fatigue-limit models and random fatigue-limit models were calibrated using normal and Weibull distributions. Here, we re-calibrate fatigue-limit models using the Birnbaum–Saunders distribution. In addition, we propose a new equivalent stress model that accommodates the different experiment types in our Dataset 1. For Dataset 2, fatigue data corresponds to rotating–bending experiments applied to round bar specimens with different sizes [33]. Again, we calibrate fatigue-limit models and compare the fit of the normal and Birnbaum–Saunders distributions. For Dataset 3, we use the laminate panel data [18,34] and calibrate and compare our proposed models.

The results show that modeling $\log(N)$ by means of the Birnbaum–Saunders distribution improves the fitting systematically in the three datasets with different variations in fatigue-limit models. It is also expected that such a choice would improve fitting with different S-N models. However, it is not our goal to find the best model for each dataset.

For Dataset 1, our proposed equivalent stress also improves data fitting using different models and distributions.

This paper is organized as follows. Section 2 considers the fatigue data of unnotched sheet specimens of 75S-T6 aluminum alloys. Six different variations of fatigue-limit models are introduced in Section 2 to show and compare stress-life models fitted to the data using the normal and Birnbaum–Saunders distributions. In Section 3, a new equivalent stress definition is proposed to eliminate the effect of the type of experiment. Section 4 presents fatigue data that correspond to unnotched round bar specimens with different sizes. Calibration and model comparison then follows in the same section. Then, laminate panel data are fitted and analyzed in Section 5 using the predefined fatigue-limit models. Conclusions are presented in Section 6.

2. Model Calibration and Comparison for Dataset 1

2.1. Description of Dataset 1

Dataset 1 consists of 85 axial-load fatigue experiments that apply constant-amplitude cyclic loading to unnotched sheet specimens of 75S-T6 aluminum alloys ([32], Table 3, pp. 22–24). These experiments were conducted at the Battelle Memorial Institute, sponsored by the National Advisory Committee for Aeronautics (NACA), to explore axial-load fatigue behavior under operational stress conditions. The data recorded for each specimen include the following:

- Maximum stress, S_{max} , measured in ksi units;
- Cycle ratio, R , defined as the minimum to maximum stress ratio. The ratio R is positive when the experiment corresponds to tension–tension loading and negative when the experiment corresponds to tension–compression loading;
- Fatigue-life, N , defined as the number of load cycles at which fatigue failure occurred; and
- A binary variable (0/1) to denote whether the test stopped before failure (run-out).

The specimen sheets have dog-bone shape with thickness of 0.09 inches, as illustrated in Figure 1. Importantly, a “critical section” is defined as the area including 1/2 inch on either side of the specimen’s minimum cross-section. Only failures occurring within this critical section were considered significant and included in the dataset. In 12 of the 85 experiments, the specimens remained unbroken when the tests were stopped. The recorded number of load cycles for these 12 experiments is the lower bound of an interval in which failure would have occurred had the test been continued. Specimens that buckled or failed outside the designated critical section are excluded from the dataset.

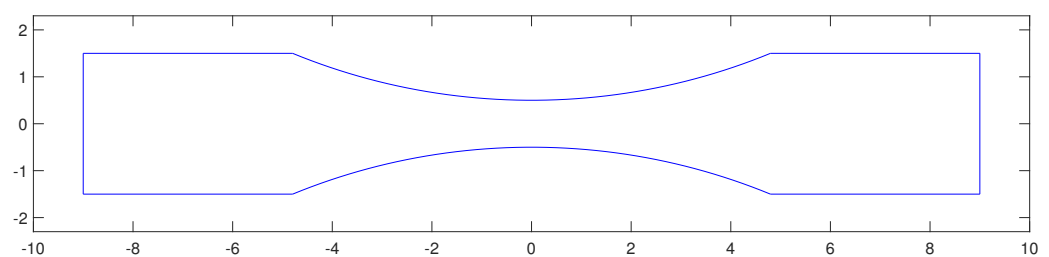


Figure 1. Shape and dimensions of sheet specimens in Dataset 1.

2.2. Fatigue-Limit Models

The fatigue-life should be modeled for a stress quantity defined for any cycle ratio. Therefore, we use Walker’s model to define the equivalent stress:

$$S_{eq} = S_{max}(1 - R)^q \quad (1)$$

where q is a fitting parameter. In the upcoming sections, we consider fatigue-limit models where the location parameter is given by $A_1 + A_2 \log_{10}(S_{eq} - A_3)$ and the fatigue-limit

parameter A_3 is a threshold parameter where fatigue-life becomes infinite when the equivalent stress is lower than A_3 . Multiple fatigue-limit models could be created based on the choice of the distribution of the fatigue-life, N . We consider three choices as follows.

2.2.1. Model Ia

In Model Ia, we assume that fatigue-life is modeled using a log-normal distribution, or equivalently, that $\log_{10}(N)$ is modeled with a normal distribution with a mean of

$$\mu(S_{eq}) = A_1 + A_2 \log_{10}(S_{eq} - A_3), \text{ if } S_{eq} > A_3 \tag{2}$$

and a constant standard deviation of $\sigma(S_{eq}) = \tau$. Moreover, fatigue experiments are assumed to be independent, and run-outs are modeled using the survival probability. Thus, the likelihood function for Model Ia is given by

$$L(A_1, A_2, A_3, \tau, q; \mathbf{n}) = \prod_{i=1}^m \left[\frac{1}{n_i \log(10)} g(\log_{10}(n_i); \mu(S_{eq}), \tau) \right]^{\delta_i} \left[1 - \Phi\left(\frac{\log_{10}(n_i) - \mu(S_{eq})}{\tau}\right) \right]^{1-\delta_i} \tag{3}$$

where $g(t; \mu, \sigma) = \frac{1}{\sqrt{2\pi}\sigma} \exp\left\{-\frac{(t-\mu)^2}{2\sigma^2}\right\}$, Φ is the cumulative distribution function of the standard normal distribution, and

$$\delta_i = \begin{cases} 1 & \text{if } n_i \text{ is a failure} \\ 0 & \text{if } n_i \text{ is a run-out} \end{cases}$$

Remark 1. Model Ia and the likelihood function (3) have been used in [16].

2.2.2. Model IIa

For Model IIa, we assume that fatigue-life is modeled using the Birnbaum–Saunders distribution, or equivalently, that $\log(N)$ is modeled with a sinh-normal distribution [31] with a constant shape parameter α , a scale parameter of 2, and a location parameter $\mu(S_{eq})$ given by Equation (2). Under this assumption, the likelihood function for Model IIa is given by

$$L(A_1, A_2, A_3, \alpha, q; \mathbf{n}) = \prod_{i=1}^m \left[\frac{1}{n_i} h(\log(n_i); \alpha, \mu(S_{eq})) \right]^{\delta_i} \left[1 - \Phi\left(\frac{2}{\alpha} \sinh\left(\frac{\log(n_i) - \mu(S_{eq})}{2}\right)\right) \right]^{1-\delta_i}$$

where $h(y; \alpha, \mu) = \frac{1}{\alpha\sqrt{2\pi}} \cosh\left(\frac{y-\mu}{2}\right) \exp\left(-\frac{2}{\alpha^2} \sinh^2\left(\frac{y-\mu}{2}\right)\right)$, $y > 0$, and $\alpha, \mu > 0$.

2.2.3. Model IIIa

For Model IIIa, we assume that $\log_{10}(N)$ is modeled using a Birnbaum–Saunders distribution with a constant shape parameter α and a location parameter $\mu(S_{eq})$, given by Equation (2). The resulting distribution for N is not the so-called log-Birnbaum–Saunders distribution reported in [31]. However, the distribution of N is obtained similarly to deriving the log-normal distribution.

$$L(A_1, A_2, A_3, \alpha, q; \mathbf{n}) = \prod_{i=1}^m \left[\frac{1}{n_i \log(10)} k(\log_{10}(n_i); \alpha, \mu(S_{eq})) \right]^{\delta_i} \left[1 - \Phi\left(\frac{1}{\alpha} \left(\sqrt{\frac{\log_{10}(n_i)}{\mu(S_{eq})}} - \sqrt{\frac{\mu(S_{eq})}{\log_{10}(n_i)}} \right) \right) \right]^{1-\delta_i}$$

where $k(y; \alpha, \mu) = \frac{1}{\sqrt{2\pi}} \frac{(y+\mu)}{2\alpha\sqrt{\mu y^{3/2}}} \exp\left\{-\frac{1}{2\alpha^2} \left(\frac{y}{\mu} + \frac{\mu}{y} - 2\right)\right\}$, $y > 0$, and $\alpha, \mu > 0$.

The three models are now fitted to Dataset 1 by maximizing the mentioned likelihood functions. Numerically, only the log-likelihood can be evaluated, and we maximize the log-likelihood instead. The ML estimates (MLEs) and the maximum log-likelihood value are reported in Table 1. The estimated parameters for Model IIa have a different scale compared with those in Models Ia and IIIa. The change in scale is only because Model IIa models

$\log(N)$ instead of $\log_{10}(N)$. However, all applied likelihood functions are normalized; therefore, the performance of the fit is not affected by the logarithm base selection.

Table 1. Maximum likelihood estimates for Models Ia, IIa, and IIIa.

	A_1	A_2	A_3	q	τ/α	Max Log-Likelihood
Model Ia	7.38	−2.01	35.04	0.5628	0.5274	−950.16
Model IIa	18.81	−5.68	33.11	0.5390	1.54	−960.68
Model IIIa	7.22	−1.90	35.32	0.5574	0.0933	−938.90

The results in Table 1 indicate that Models Ia and IIIa provide the best fit for Dataset 1. We visualize the fit using the 0.05 and 0.95 quantile functions and the median function. The data can also be plotted given the MLE of q . We distinguish data based on the experiment type or stress ratio. Figures 2 and 3 illustrate the quantile functions of Models Ia and IIIa obtained using the MLE parameters. The quantile functions of Model IIIa produce a better fit than those of Model Ia, which coincides with the fact that Model IIIa has the highest log-likelihood value among the three models in Table 1. We also observe that data seem segregated by the median according to the experiment type: tension–tension ($R > 0$) and tension–compression ($R < 0$). We analyze this behavior further in Section 3.

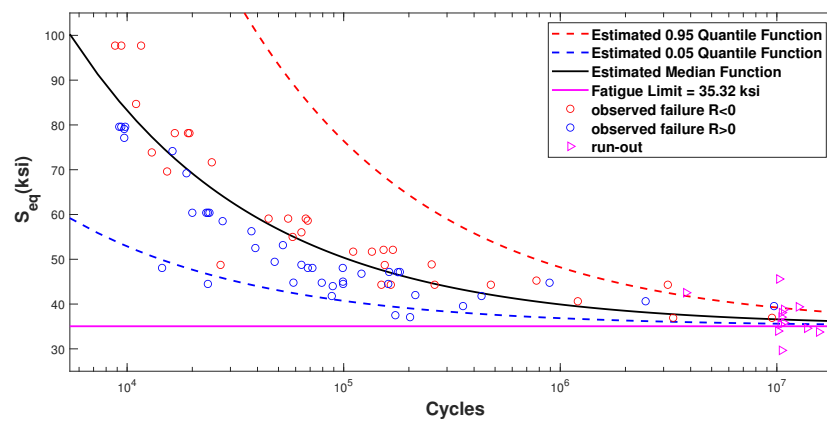


Figure 2. Model Ia: $\log_{10}(N) \sim N(\mu(S_{eq}), \sigma)$ and $S_{eq} = S_{max}(1 - R)^q$.

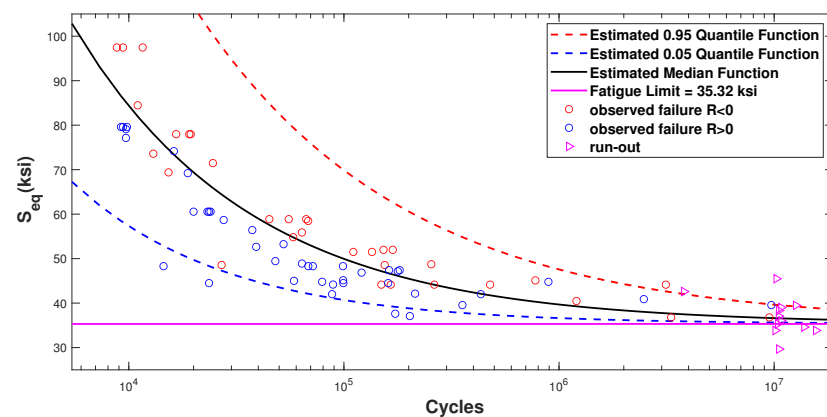


Figure 3. Model IIIa: $\log_{10}(N) \sim BS(\alpha, \mu(S_{eq}))$ and $S_{eq} = S_{max}(1 - R)^q$.

We allow the standard deviation or shape parameter to be non-constant to improve the fit of the three previous models. In particular, we assume this parameter is a function of the equivalent stress. With the same probability distributions previously considered, we introduce three new fatigue-limit models with non-constant standard deviation/shape parameters.

2.2.4. Model Ib

Analogous to Model Ia, for Model Ib, we assume that $\log_{10}(N)$ has a normal distribution with the mean function $\mu(S_{eq})$ defined in Equation (2). However, the standard deviation is assumed to be non-constant and given by $\sigma(S_{eq}) = 10^{(B_1+B_2 \log_{10}(S_{eq}))}$. The resulting likelihood function is equivalent to that derived for Model Ia.

2.2.5. Model IIb

For Model IIb, the fatigue-life N is modeled by the Birnbaum–Saunders distribution with location parameter $\mu(S_{eq})$ (defined in Equation (2)) and non-constant shape parameter $\alpha(S_{eq}) = 10^{(B_1+B_2 \log_{10}(S_{eq}))}$.

2.2.6. Model IIIb

For Model IIIb, $\log_{10}(N)$ is modeled using the Birnbaum–Saunders distribution with the location parameter $\mu(S_{eq})$ and non-constant shape parameter $\alpha(S_{eq}) = 10^{(B_1+B_2 \log_{10}(S_{eq}))}$.

The new Models Ib, IIb, and IIIb are calibrated to fit Dataset 1, and the MLEs of the parameters of these models are presented in Table 2. Comparing the maximum log-likelihood values in Tables 1 and 2 reveals that the fit improved considerably for all models. In contrast, the difference between the new models decreased, with Model IIIb still providing the best fit.

Table 2. Maximum likelihood estimates for Models Ib, IIb, and IIIb.

	A_1	A_2	A_3	q	B_1	B_2	Max Log-Likelihood
Model Ib	6.72	−1.57	36.21	0.5510	4.55	−2.89	−920.51
Model IIb	16.56	−4.26	35.51	0.5239	5.54	−3.21	−926.97
Model IIIb	6.70	−1.56	36.24	0.5501	2.90	−2.34	−917.38

We compare the fit of Models Ib and IIIb using the quantile functions in Figures 4 and 5. Both models produced significantly improved fit compared with Figures 2 and 3. The fatigue-limit parameter slightly increased, and the 0.05 quantile converges rapidly to its asymptote as the equivalent stress approaches the fatigue-limit. In both cases, the data remain mostly partitioned by the median into the two experiment types.

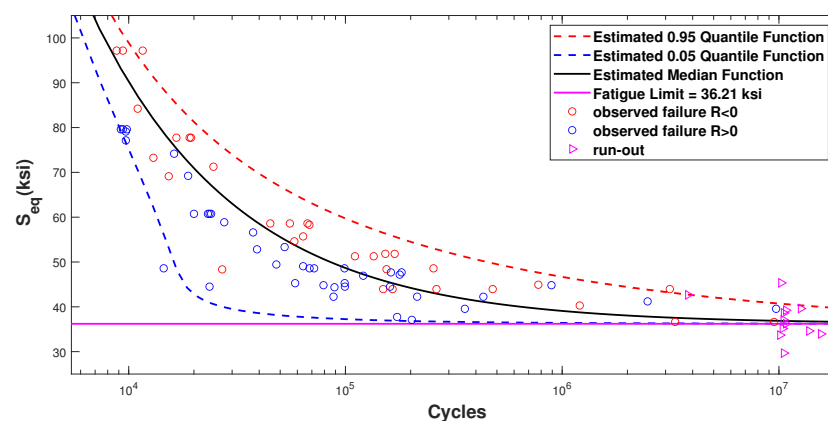


Figure 4. Model Ib: $\log_{10}(N) \sim N(\mu(S_{eq}), \sigma(S_{eq}))$ and $S_{eq} = S_{max}(1 - R)^q$.

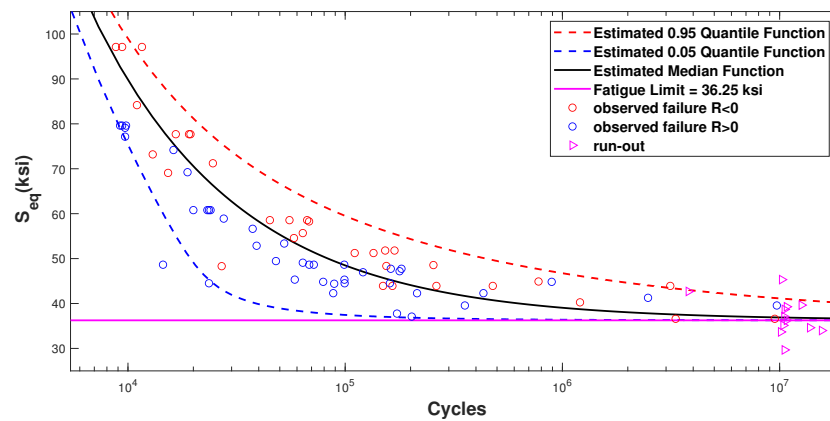


Figure 5. Model IIIb: $\log_{10}(N) \sim BS(\alpha(S_{eq}), \mu(S_{eq}))$ and $S_{eq} = S_{max}(1 - R)^q$.

2.3. Model Comparison

Using a classical approach, we compute some popular information criteria, such as the Akaike information criterion (AIC) [35], Bayesian information criterion (BIC) [36,37], and AIC with correction [38], which are based on the maximized log-likelihood values. Such measures consider the goodness of fit and complexity of the models regarding the number of parameters. Table 3 contains the maximum log-likelihood values corresponding to the models introduced in Section 2.2 and the classical information criterion computations.

Table 3. Classical information criteria.

Models	Ia	Ib	IIa	IIb	IIIa	IIIb
Maximum log-likelihood	−950.16	−920.51	−960.68	−926.97	−938.90	−917.38
Akaike information criterion (AIC)	1910.3	1853.0	1931.4	1865.9	1887.8	1846.8
Bayesian information criterion (BIC)	1922.5	1867.7	1943.6	1880.6	1900.0	1861.4
Akaike information criterion with correction	1911.1	1854.1	1932.1	1867.0	1888.5	1847.8

3. Analysis of the Stress Ratio Effect and Equivalent Stress for Dataset 1

In all previous models, the equivalent stress is based on Walker’s model [39], which is $S_{max}(1 - R)^q$. The following analysis in Table 4 reveals that the parameter q is related to the sign of the cycle ratio R .

Table 4. Maximum likelihood estimates for Models I and II with $S_{eq} = S_{max}(1 - R)^q$.

Model	Data	A_1	A_2	A_3	q	$\tau/\alpha/B_1$	B_2	Max Log-Likelihood
Ia	$R < 0$	7.94	−2.10	61.43	1.37	0.3203	—	−403.56
IIIa	$R < 0$	7.89	−2.10	57.643	1.2753	0.0575	—	−399.64
Ib	$R < 0$	7.44	−1.86	52.56	1.12	5.23	−3.09	−392.86
IIIb	$R < 0$	7.41	−1.85	52.06	1.0986	3.40	−2.50	−392.23
Ia	$R > 0$	6.93	−1.84	34.86	0.6304	0.5561	—	−531.21
IIIa	$R > 0$	6.75	−1.71	35.18	0.6269	0.0974	—	−523.95
Ib	$R > 0$	6.84	−1.75	36.55	0.5410	8.11	−5.07	−500.46
IIIb	$R > 0$	6.75	−1.69	36.62	0.5388	6.27	−4.41	−499.15

In Table 4, the fatigue-limit parameter, A_3 , has a different scale based on the stress ratio. We divided $1 - R$ by 2 in the equivalent stress formula to solve this. However, the estimated values of q do not change. Therefore, we defined the equivalent stress as $S_{max}(\frac{1-R}{2})^{1+q}$

or $S_a(\frac{1-R}{2})^q$, where S_a denotes the stress amplitude. Then, we recalibrated the proposed models in Table 5. The fatigue-limit parameter has the same scale for $R > 0$ and $R < 0$. In contrast, the estimated value of q changes signs with R . Thus, it seems reasonable to propose the following equivalent stress:

$$S_{eq} = S_{max} \left(\frac{1-R}{2} \right)^{1-\text{sign}(R)q} \tag{4}$$

Table 5. Maximum likelihood estimates for Models I and II with $S_{eq} = S_{max}(\frac{1-R}{2})^{1+q}$.

Model	Data	A_1	A_2	A_3	q	$\tau/\alpha/B_1$	B_2	Max Log-Likelihood
Ia	$R < 0$	7.08	-2.11	23.80	0.3679	0.3203	—	-403.56
IIIa	$R < 0$	7.09	-2.10	23.81	0.2754	0.0575	—	-399.64
Ib	$R < 0$	6.82	-1.86	24.26	0.1156	4.19	-3.09	-392.86
IIIb	$R < 0$	6.80	-1.85	24.31	0.0986	2.57	-2.50	-392.23
Ia	$R > 0$	6.59	-1.84	22.52	-0.3696	0.5561	—	-531.21
IIIa	$R > 0$	6.43	-1.71	22.78	-0.3732	0.0974	—	-523.95
Ib	$R > 0$	6.56	-1.75	25.12	-0.4590	7.29	-5.07	-500.46
IIIb	$R > 0$	6.54	-1.74	25.19	-0.4607	5.68	-4.49	-499.13

Next, we calibrate the parameters using the full data ($R > 0$ and $R < 0$). Table 6 presents the MLEs of Models Ia, IIIa, Ib, and IIIb, along with the maximum log-likelihood and AIC values. The fit is considerably improved in all cases using the equivalent stress Equation (4).

Table 6. Maximum likelihood estimates for Models I and II with $S_{eq} = S_{max}(\frac{1-R}{2})^{1-\text{sign}(R)q}$.

Model	A_1	A_2	A_3	q	$\tau/\alpha/B_1$	B_2	Max Log-Likelihood	AIC
Ia	6.99	-2.09	23.72	0.4310	0.4797	—	-942.55	1895.1
IIIa	6.81	-1.95	23.98	0.4336	0.0845	—	-930.85	1871.7
Ib	6.58	-1.76	24.56	0.4433	5.97	-4.23	-899.36	1810.7
IIIb	6.54	-1.74	24.62	0.4436	4.38	-3.65	-897.67	1807.3

Figures 6 and 7 illustrate the new quantile functions of Models Ia and IIIa with improved equivalent stress Equation (4). The variance is reduced compared to quantiles in Figures 2 and 3. In addition, the two data types are well distributed around the median. Furthermore, the fit can be slightly improved by adapting Huang’s model [40] for $R > 0.5$. For Models Ib and IIIb, the estimated quantile functions with the new equivalent stress are presented in Figures 8 and 9.

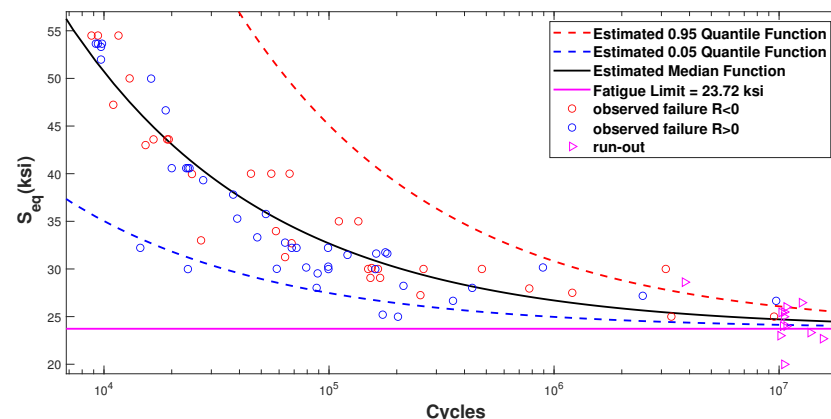


Figure 6. Model Ia: $\log_{10}(N) \sim N(\mu(S_{eq}), \sigma)$ and $S_{eq} = S_{max}(\frac{1-R}{2})^{1-\text{sign}(R)q}$.

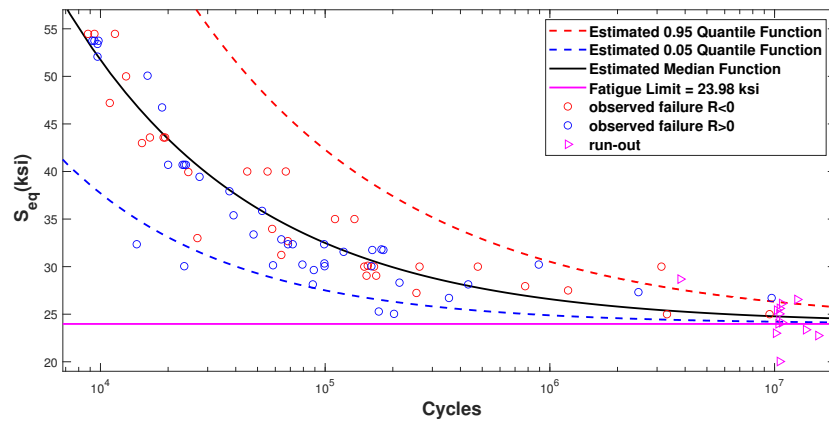


Figure 7. Model IIIa: $\log_{10}(N) \sim BS(\alpha, \mu(S_{eq}))$ and $S_{eq} = S_{max}(\frac{1-R}{2})^{1-\text{sign}(R)q}$.

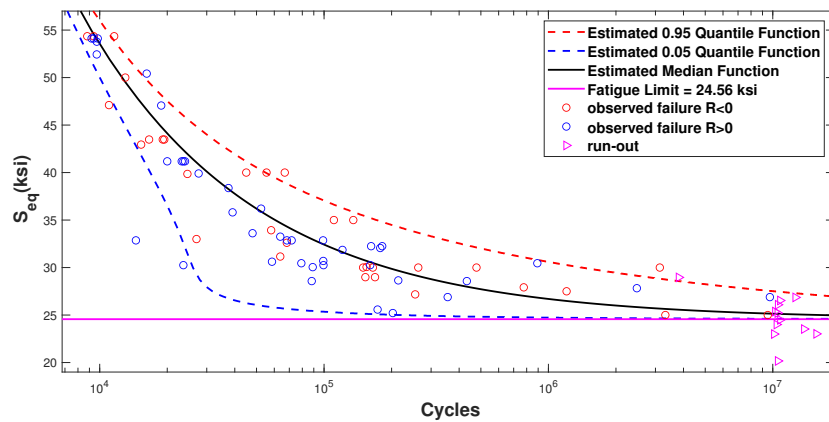


Figure 8. Model Ib: $\log_{10}(N) \sim N(\mu(S_{eq}), \sigma(S_{eq}))$ and $S_{eq} = S_{max}(\frac{1-R}{2})^{1-\text{sign}(R)q}$.

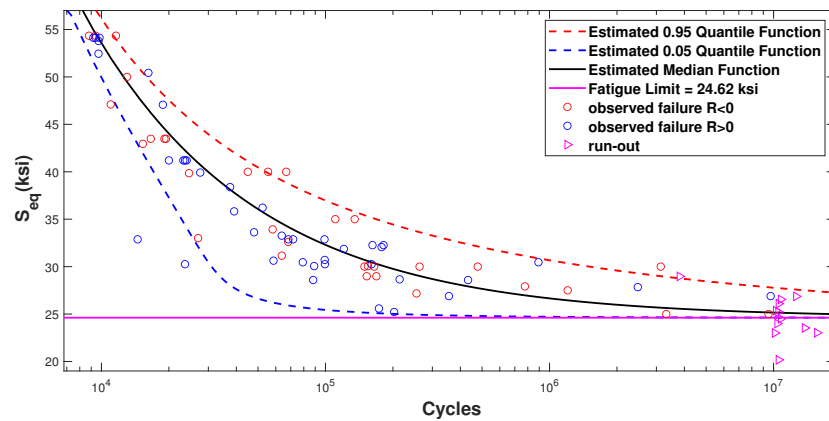


Figure 9. Model IIIb: $\log_{10}(N) \sim BS(\alpha(S_{eq}), \mu(S_{eq}))$ and $S_{eq} = S_{max}(\frac{1-R}{2})^{1-\text{sign}(R)q}$.

3.1. Profile Likelihood

We compare the profile likelihood of the fatigue-limit obtained using the previous models. Figure 10 depicts the profile likelihood of the fatigue-limit, A_3 , using Models Ia and IIIa. For constant variance and shape parameters, the estimated profile likelihood using the Birnbaum–Saunders distribution (Model IIIa) has a noticeably higher mode and a lower variance than Model Ia, which uses the normal distribution. When adopting non-constant variance and shape parameters, the difference between the two profile likelihoods is negligible, as displayed in Figure 11.

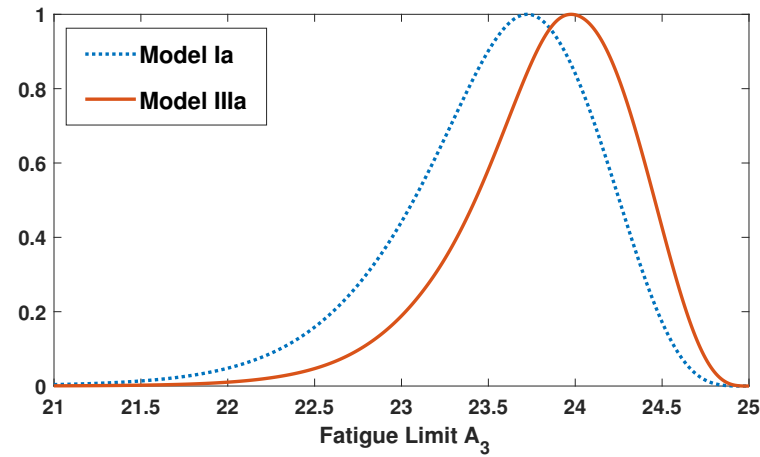


Figure 10. Profile likelihoods of the fatigue-limit parameters using Models Ia and IIIa.

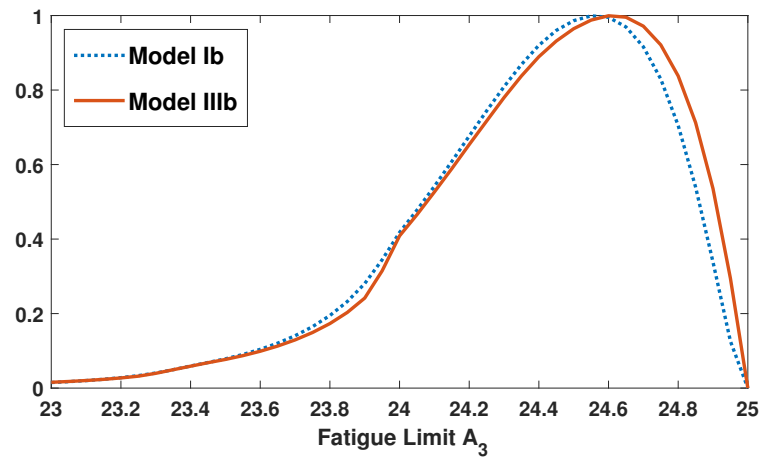


Figure 11. Profile likelihoods of the fatigue-limit parameters using Models Ib and IIIb.

3.2. Survival Functions

We closely examined the survival functions obtained by calibrated Models Ia, Ib, IIIa, and IIIb at different values of S_{max} and R in Figure 12. The Birnbaum–Saunders model (Model IIIa) outperformed the counterpart Gaussian model (Model Ia) because it offers a higher survival probability before the observed failure and a lower survival probability after the observed failure. For Models IIIa and IIIb, the resulting survival probabilities are almost identical for both distributions.

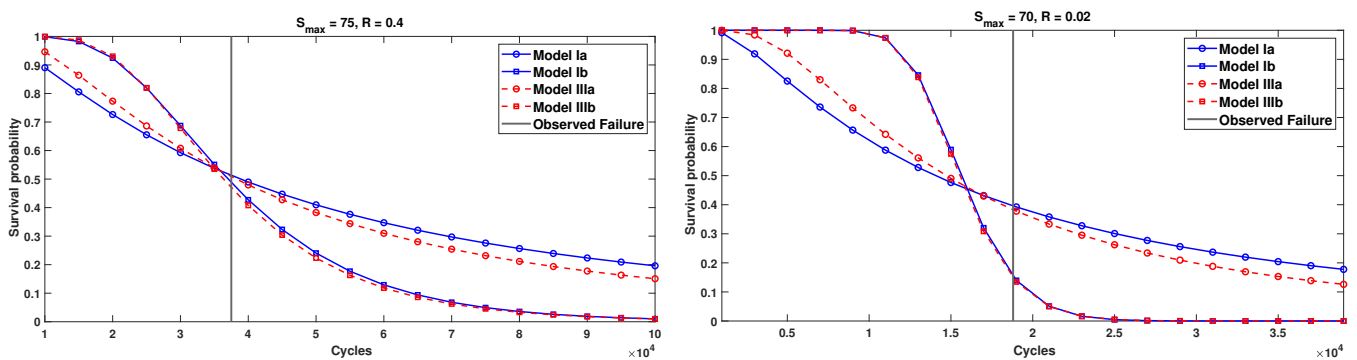


Figure 12. Cont.

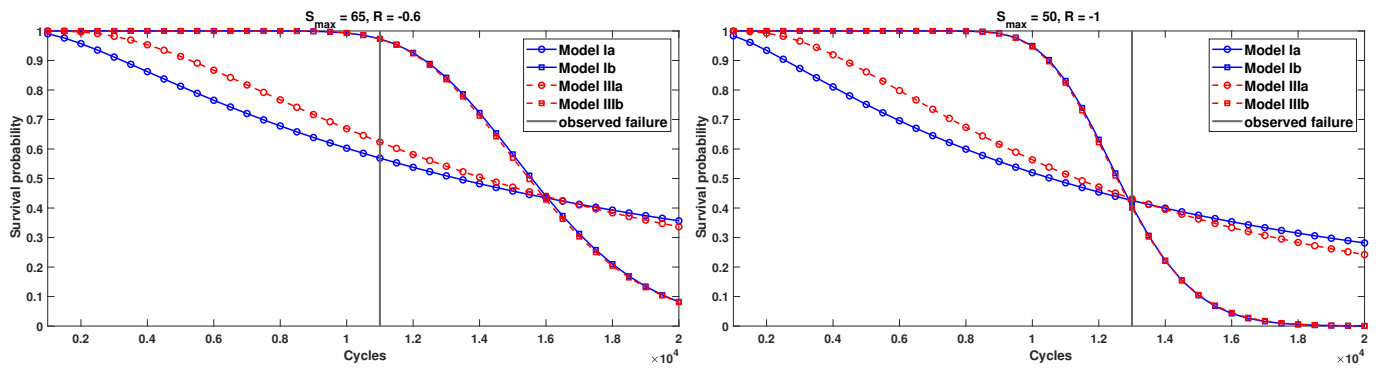


Figure 12. Survival functions of Dataset 1 specimens using calibrated Models Ia, Ib, IIIa, and IIIb for different values of S_{max} and R .

4. Model Calibration and Comparison for Dataset 2

4.1. Description of Dataset 2

This section introduces new datasets for unnotched specimens of 75S-T6 aluminum alloys. This dataset encompasses the results of the rotating–bending fatigue experiments conducted on 101 round bar specimens, showcasing five different minimum-section diameters; namely, the diameters are 1/8 inch, 1/4 inch, 1/2 inch, 1 inch, and 1 3/4 inches, as reported in Tables 6 to 10 in the technical note [33]. The stress ratio for these experiments is set at -1 , indicating fully reversed loading conditions. Among the total specimens, 13 experiments were classified as run-outs, where the specimens did not fail within the test duration. The distribution of unnotched specimens across the five different minimum-section diameters and the corresponding number of run-outs for each category are summarized in Table 7.

Table 7. Number of unnotched specimens and run-outs for each round bar diameter.

Minimum-Section Diameter (Inches)	Number of Unnotched Specimens	Number of Run-Outs
1/8	32	3
1/4	28	5
1/2	14	2
1	17	3
1 3/4	10	0

Similar to Dataset 1, these fatigue tests were performed at the Battelle Memorial Institute, under the sponsorship of the National Advisory Committee for Aeronautics. The 75S-T6 aluminum alloy was selected due to its importance in aircraft design. The samples were cut from 3 inch diameter round bars sourced from the Aluminum Company of America. To maintain consistency among specimens of various sizes for fatigue testing, a specific surface finish was carefully chosen. This involved mechanical polishing and an electrolytic polish to reduce surface-related differences in fatigue behavior.

Again, we consider fatigue-limit Models Ia, Ib, IIIa, and IIIb with the new equivalent stress Equation (4) to fit the data introduced in Section 4.1. As mentioned, the stress ratio for rotating–bending experiments is -1 ; therefore, the equivalent stress equals S_{max} .

Table 8 provides the MLEs for Models Ia, Ib, IIIa, and IIIb when separately fitting Specimens 1 and 2. The joint fit for all specimens is also provided. The goodness of fit and estimated fatigue-limit decreased when the data were combined. Figures 13 and 14 reveal the quantiles of calibrated Models Ia and Ib, respectively.

Table 8. Maximum likelihood estimates for Models I and III with $S_{eq} = S_{max}$.

Model	Specimen	Diameter	A_1	A_2	A_3	$\tau/\alpha/B_1$	B_2	Max Log-Likelihood
Ia	1	1/8	7.20	−1.73	21.17	0.4420	—	−428.28
Ib	1	1/8	7.36	−1.87	21.11	2.38	−1.87	−425.73
IIIa	1	1/8	7.17	−1.72	21.23	0.0721	—	−426.06
IIIb	1	1/8	7.28	−1.82	21.21	0.88	−1.38	−424.62
Ia	2	1/4	8.21	−2.69	21.86	0.4002	—	−343.94
Ib	2	1/4	7.21	−1.86	22.88	8.70	−6.33	−327.49
IIIa	2	1/4	7.96	−2.48	22.16	0.0604	—	−340.75
IIIb	2	1/4	7.20	−1.85	22.91	6.86	−5.62	−326.85
Ia	All	—	9.03	−3.04	18.68	0.5626	—	−1357.8
Ib	All	—	8.23	−2.50	20.49	3.39	−2.53	−1338.1
IIIa	All	—	8.73	−2.84	19.24	0.0880	—	−1349.6
IIIb	All	—	8.15	−2.45	20.61	1.86	−2.02	−1336.1

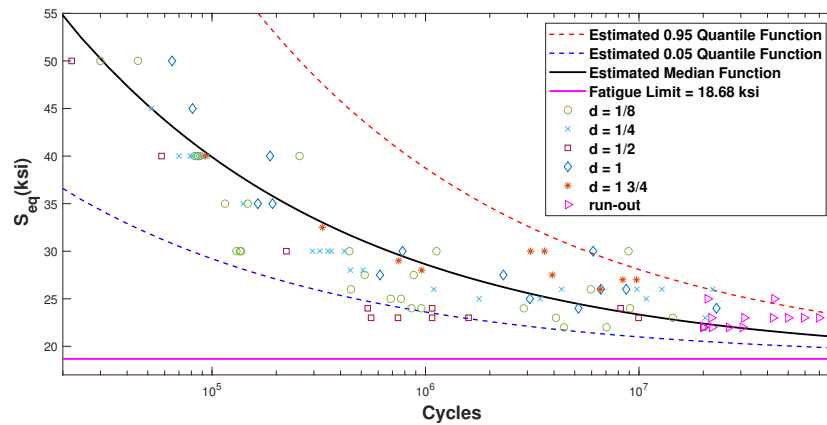


Figure 13. Model Ia: $\log_{10}(N) \sim N(\mu(S_{eq}), \sigma)$ and $S_{eq} = S_{max}$.

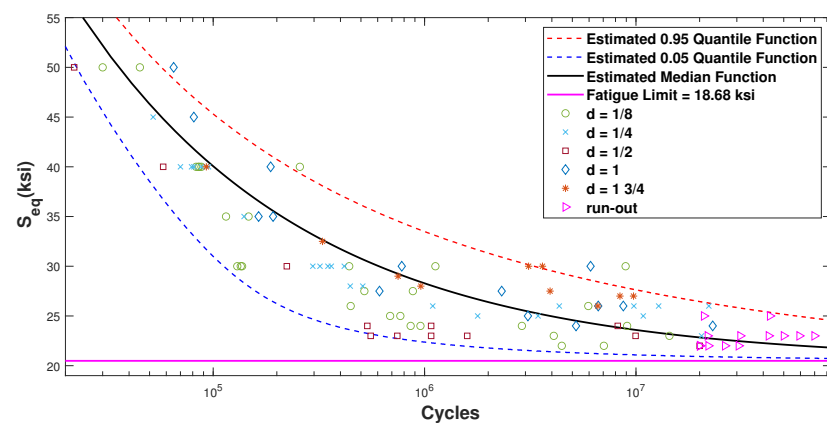


Figure 14. Model Ib: $\log_{10}(N) \sim N(\alpha(S_{eq}), \mu(S_{eq}))$ and $S_{eq} = S_{max}$.

4.2. Profile Likelihood and Confidence Intervals

We again compare the profile likelihood of the fatigue-limit obtained from the four previous models using Dataset 2. Figure 15 displays the profile likelihood of the fatigue-limit, A_3 , using Models Ia and IIIa. As concluded, the profile likelihood when using the Birnbaum–Saunders distribution (Model IIIa) has a higher mode and much lower

variance than Model Ia. With non-constant variance and shape parameters, the two profile likelihoods are almost identical Figure 16.

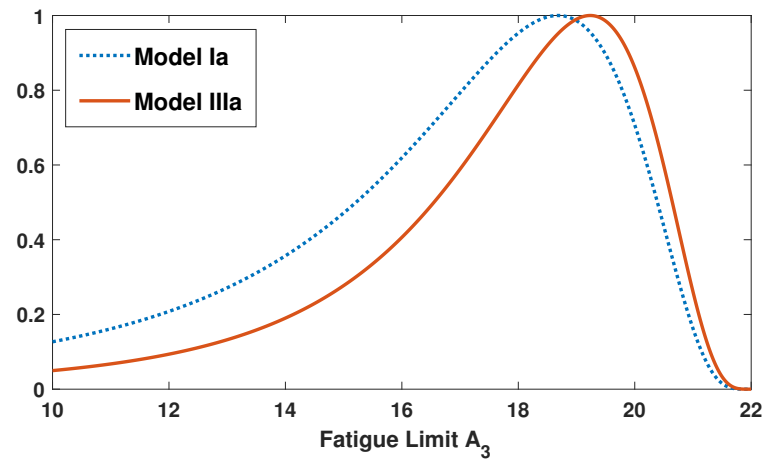


Figure 15. Profile likelihoods of the fatigue-limit parameters using Models Ia and IIIa.

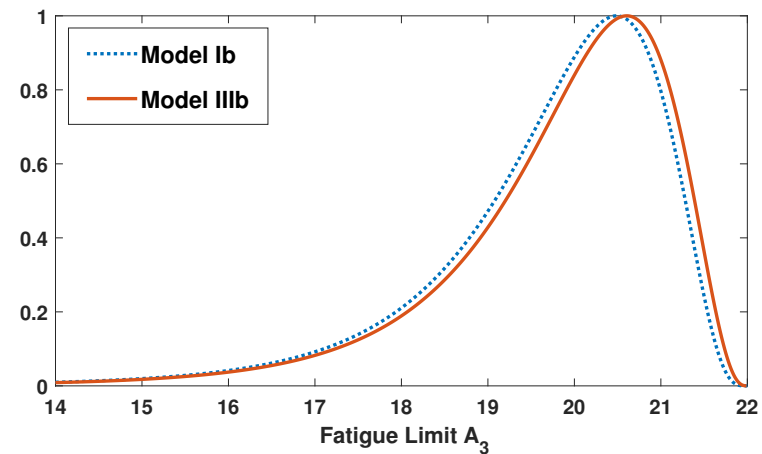


Figure 16. Profile likelihoods of the fatigue-limit parameters using Models Ib and IIIb.

We confirmed the mentioned conclusions by estimating the confidence intervals of the pooled MLEs, given that Dataset 2 is complete. The confidence intervals presented in Table 9 are obtained by stratified bootstrapping, where the sampled dataset maintains the same proportions in the original data related to the five specimens. The results indicate that the Birnbaum–Saunders distribution provides tighter confidence intervals than the normal distribution, especially when using a constant variance. This property is essential to generate accurate survival and failure predictions.

Table 9. Confidence intervals of 90% for the pooled maximum likelihood estimates for Models I and III.

Model	A_1	A_2	A_3	$\tau/\alpha/B_1$	B_2
Ia	(7.9, 11.1)	(−4.3, −2.2)	(14.3, 21)	(0.49, 0.62)	—
Ib	(7.6, 9.2)	(−3.1, −2.1)	(18.5, 21.6)	(2.8, 4.6)	(−3.4, −2.1)
IIa	(7.8, 10.3)	(−3.8, −2.2)	(15.7, 21.1)	(0.077, 0.096)	—
IIb	(7.6, 9.1)	(−3.1, −2.0)	(18.6, 21.7)	(1.3, 3)	(−2.9, −1.6)

4.3. Survival Functions

Figure 17 depicts the survival probabilities of specimens from Dataset 2 under different settings using calibrated models by the pooled or specific specimen data.

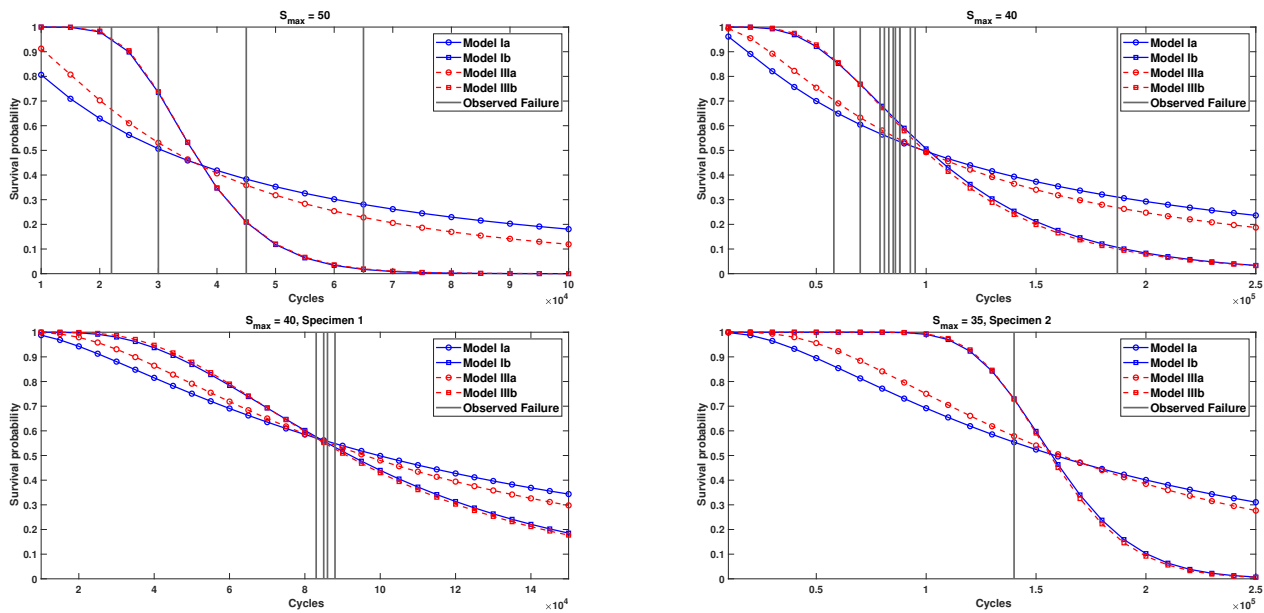


Figure 17. Survival functions of Dataset 2 specimens using calibrated Models Ia, Ib, IIIa, and IIIb for values of S_{max} and R .

Comparing the results for Datasets 1 and 2, we notice higher variability in the latter, especially when using pooled Dataset 2 with multiple specimens of different geometries and sizes. The fit results could be improved using Poisson models that consider the geometry and size of the specimen [41]. However, implementing and analyzing such models is beyond the scope of the current work.

5. Model Calibration and Comparison for Dataset 3

Description of Dataset 3

To generalize the previous results, we consider a well-known dataset: the laminate panel S-N dataset [18,34]. This dataset contains fatigue data for 125 carbon eight-harness-satin/epoxy laminate specimens subjected to four-point out-of-plane bending tests, where 10 out of 125 experiments are run-outs. In this case, the equivalent stress needed in the fatigue-limit models is given directly in the data, and we do not have the stress ratio. Recent studies such as [42,43] have used this dataset to validate and test new models to predict fatigue life.

As a first illustration, we use probability plots, as suggested in [43]. Figures 18 and 19 present the probability plot of the normal distribution and Birnbaum–Saunders distribution as models for the fatigue-life, N . Modeling N using the normal or Birnbaum–Saunders distribution is not a good choice. Instead, modeling $\log(N)$ using these distributions provides better probability plots, as illustrated in Figures 20 and 21.

We calibrate six fatigue-limit models, Ia, Ib, IIa, IIb, IIIa, and IIIb, slightly modified using natural instead of base 10 logarithms. This approach is conducted to make the MLE parameters comparable to the results in the literature and does not affect the goodness of fit. We also fit the data using the Weibull distribution but do not include these results, as this distribution consistently provides the worst fit.

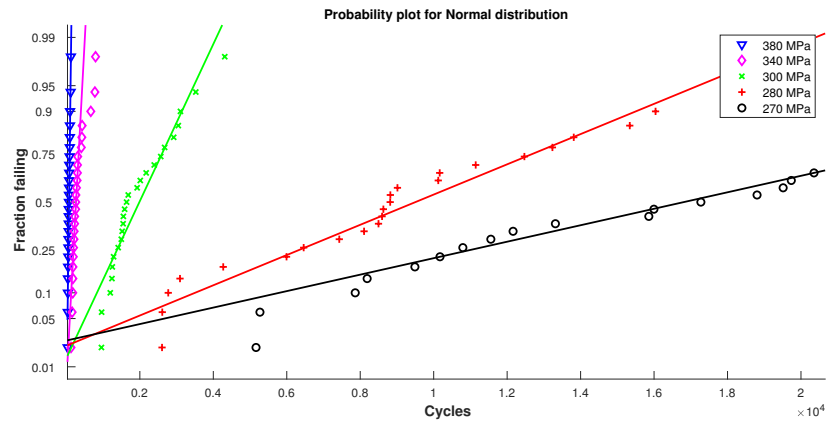


Figure 18. Probability plot of the normal distribution as a model for the number of cycles N .

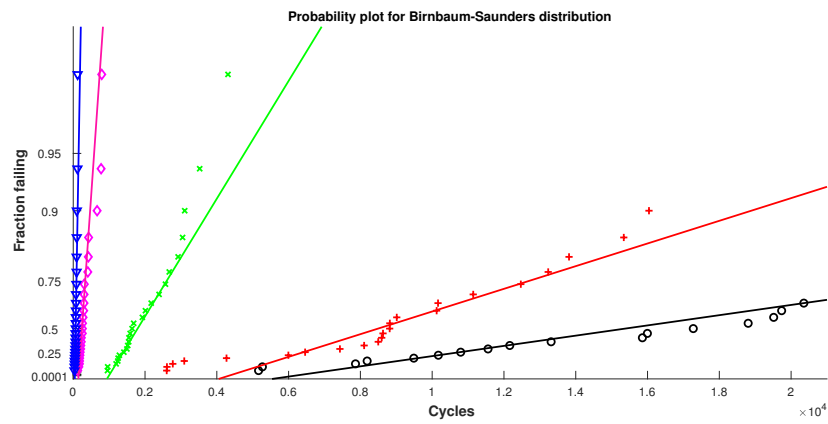


Figure 19. Probability plot of the Birnbaum–Saunders distribution as a model for the number of cycles N .

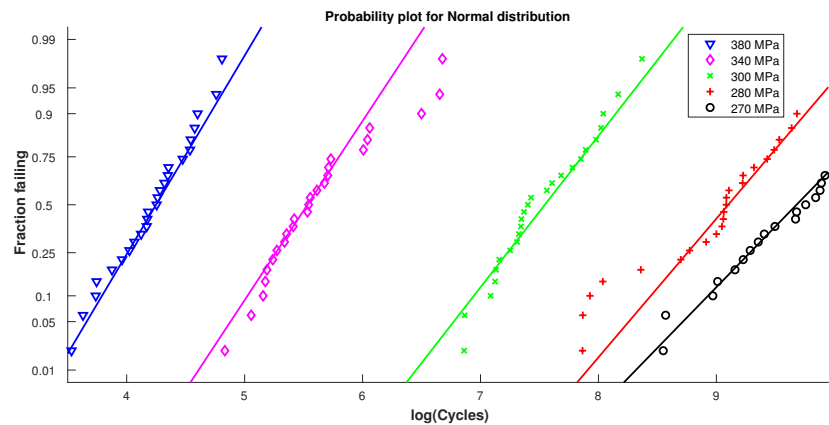


Figure 20. Probability plot of the normal distribution as a model for $\log(N)$.

Table 10 provides the MLEs for Models Ia, Ib, IIa, IIb, IIIa, and IIIb. Table 11 compares all six models employing classical information criteria. Figures 22 and 23 present the quantiles of calibrated Models Ia and IIIa, respectively. Figures 24 and 25 display the quantiles of calibrated Models Ib and IIIb, respectively.

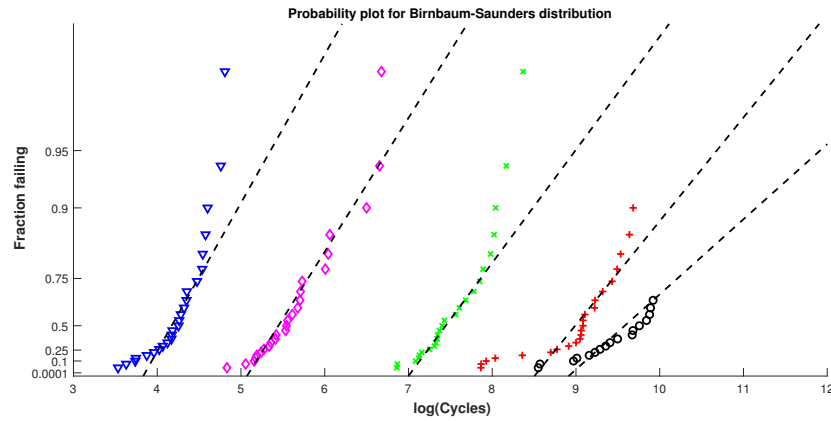


Figure 21. Probability plot of the Birnbaum–Saunders distribution as a model for $\log(N)$.

Table 10. Maximum likelihood estimates for Models I, II, and III.

Model	A_1	A_2	A_3	$\tau/\alpha/B_1$	B_2	Max Log-Likelihood
Ia	31.56	−5.32	209.69	0.4902	—	−889.77
Ib	30.26	−5.10	214.22	8.71	−1.64	−885.28
IIa	32.15	−5.43	207.55	0.5031	—	−889.90
IIb	30.77	−5.18	212.45	9.01	−1.69	−885.17
IIIa	29.63	−4.99	216.48	0.0718	—	−885.64
IIIb	30.14	−5.08	214.59	−6.84	0.73	−884.67

Table 11. Classical information criteria.

Models	Ia	Ib	IIa	IIb	IIIa	IIIb
Maximum log-likelihood	−889.77	−885.28	−889.90	−885.17	−885.64	−884.67
Akaike information criterion (AIC)	1787.5	1780.6	1787.8	1780.3	1779.3	1779.3
Bayesian information criterion (BIC)	1798.9	1794.7	1799.1	1794.5	1790.6	1793.5
Akaike information criterion with correction	1787.9	1781.1	1788.1	1780.8	1779.6	1779.8

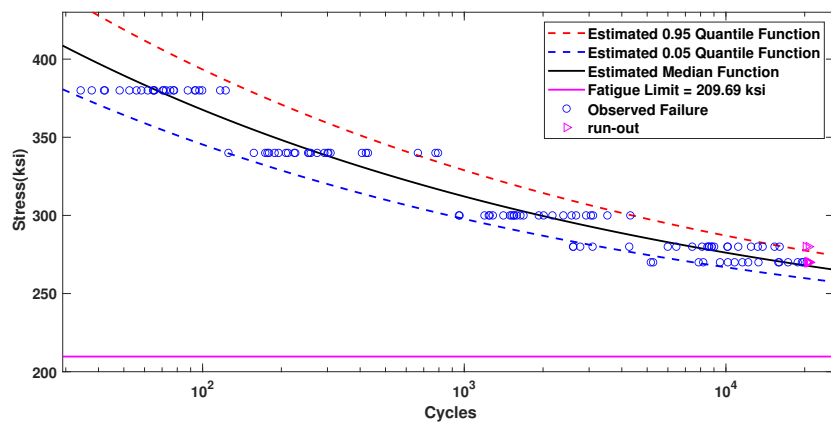


Figure 22. Model Ia: $\log(N) \sim N(\mu(S), \sigma)$.

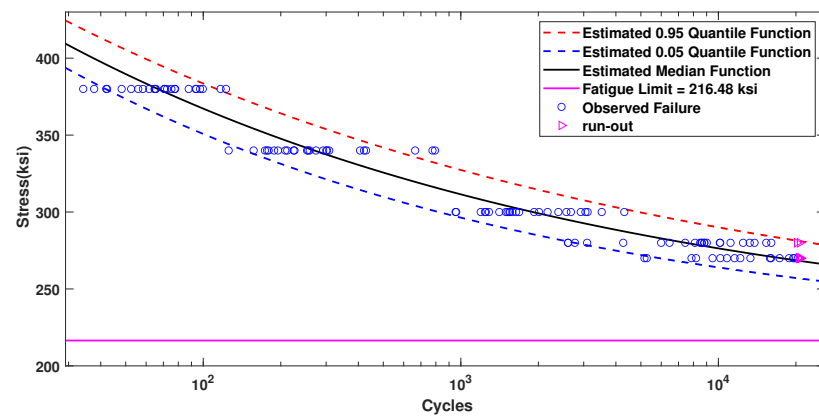


Figure 23. Model IIIa: $\log(N) \sim BS(\alpha, \mu(S))$.

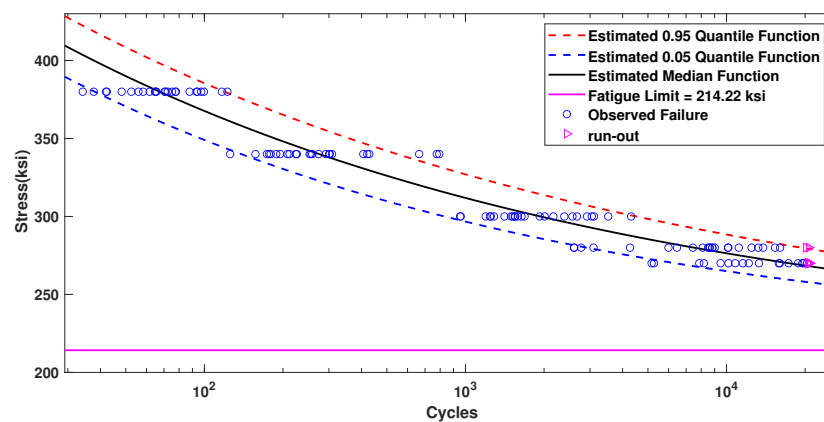


Figure 24. Model Ib: $\log(N) \sim N(\mu(S), \sigma(S))$.

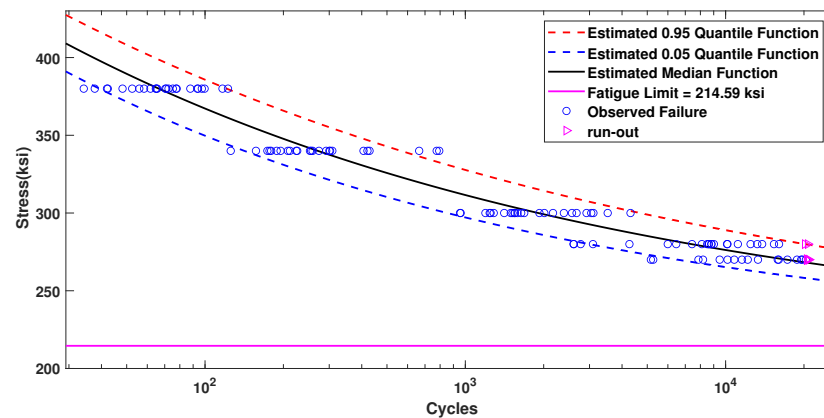


Figure 25. Model IIIb: $\log(N) \sim BS(\alpha(S), \mu(S))$.

6. Conclusions

Multiple variants of the fatigue-limit models were calibrated and ranked employing ML and classical information criteria. The proposed approach of modeling the logarithm of the fatigue-life using the Birnbaum–Saunders distribution proved to be superior or equivalent to the best model in all cases.

For Dataset 1, fatigue experiments included two types of loadings. We introduced a new equivalent stress to generalize the models for such scenarios. Therefore, the fit for Dataset 1 considerably improved for all models. The suggested equivalent stress does not require adding new parameters and could be used for fatigue data with only one loading type.

In Dataset 2, five types of round bar specimens were subjected to rotating–bending fatigue experiments. The calibration was performed using Specimens 1 and 2 individually.

Then, pooled calibration was performed using the full dataset. The variability of the latter calibration increased, which was further analyzed by obtaining confidence intervals of the MLEs via bootstrapping.

Laminate panel data were adopted in Section 5. Models I, II, and III were calibrated and ranked using constant and non-constant variance/shape parameters. The fit results confirmed that Birnbaum–Saunders models are better than log-normal and Weibull models, especially when the variance is constant. Model IIIa is preferable over IIIb when comparing the classical information criteria.

For all calibrated models, we analyzed the data with the estimated S-N curves and survival probabilities in the three datasets. The various models were compared using AIC, BIC, and AIC with correction. Profile likelihoods were also computed for the fatigue-limit parameter.

The Birnbaum–Saunders distribution provided a better fit for data and higher confidence in estimating the fatigue-limit parameter in Model IIIa. Models Ib and IIIb yielded similar results regarding information criteria, survival probabilities, and profile likelihood. A non-constant variance with the log-normal distribution could be an alternative to the proposed Birnbaum–Saunders model in some frameworks.

Our study demonstrates that the Birnbaum–Saunders distribution, when employed to model the logarithm of the fatigue-life, surpasses the predictive accuracy of traditional models. This advantage is particularly pronounced in scenarios involving complex stress-loading conditions, where the flexibility of the Birnbaum–Saunders distribution enables a more detailed understanding of fatigue-life expectancy.

We reiterate that this study is academic and focused on the crack initiation stage of fatigue-life in controlled and homogeneous specimen environments. The datasets employed assume that the specimens possess uniform material properties and surface finishes. Consequently, the findings and probability distributions derived from our analysis may not directly reflect those observed in operational components with varying quality and environmental exposure. In real-world scenarios, the presence of initial damages, such as equivalent initial damage size (EIDS), should be carefully considered. This would require more extensive data and detailed information about the operational components to ensure meaningful results.

For future directions in this research, there is significant potential to expand the application of Birnbaum–Saunders distributions beyond the scope of S-N models to crack propagation and damage tolerance models. Traditionally, these areas have often utilized log-normal or Weibull distributions [44]. Furthermore, considering the effects of environmental factors such as corrosion, as discussed in [45,46], could enrich the predictive capabilities of these models. These types of studies could offer a more comprehensive insight into fatigue and fracture in working conditions where accurate predictions are essential for the maintenance and safety of mechanical systems.

Author Contributions: Conceptualization, Z.S. and M.S.; Methodology, Z.S. and M.S.; Software, Z.S.; Validation, R.T.; Formal analysis, Z.S.; Investigation, M.S.; Resources, R.T.; Data curation, Z.S.; Writing—original draft, Z.S.; Writing—review & editing, M.S. and R.T.; Visualization, Z.S.; Project administration, R.T. All authors have read and agreed to the published version of the manuscript.

Funding: This research received no external funding.

Data Availability Statement: The original contributions presented in the study are included in the article, further inquiries can be directed to the corresponding author.

Acknowledgments: This paper is based upon work supported by King Fahd University of Petroleum & Minerals.

Conflicts of Interest: The authors declare no conflict of interest.

References

1. Schijve, J. Fatigue of structures and materials in the 20th century and the state of the art. *Int. J. Fatigue* **2003**, *25*, 679–702. [[CrossRef](#)]
2. Schijve, J. *Fatigue of Structures and Materials*, 2nd ed.; Springer: Berlin/Heidelberg, Germany, 2009.
3. Fatemi, A.; Yang, L. Cumulative fatigue damage and life prediction theories: A survey of the state of the art for homogeneous materials. *Int. J. Fatigue* **1998**, *20*, 9–34. [[CrossRef](#)]
4. Murakami, Y.; Takagi, T.; Wada, K.; Matsunaga, H. Essential structure of SN curve: Prediction of fatigue life and fatigue limit of defective materials and nature of scatter. *Int. J. Fatigue* **2021**, *146*, 106138. [[CrossRef](#)]
5. Askes, H.; Susmel, L. Understanding cracked materials: Is linear elastic fracture mechanics obsolete? *Fatigue Fract. Eng. Mater. Struct.* **2015**, *38*, 154–160. [[CrossRef](#)]
6. He, H.; Liu, H.; Mura, A.; Zhu, C. Gear bending fatigue life prediction based on continuum damage mechanics and linear elastic fracture mechanics. *Meccanica* **2023**, *58*, 119–135. [[CrossRef](#)]
7. Yue, F.; Wu, Z. Fracture mechanical analysis of thin-walled cylindrical shells with cracks. *Metals* **2021**, *11*, 592. [[CrossRef](#)]
8. Rahim, M.R.B.A.; Schmauder, S.; Manurung, Y.H.; Binkele, P.; Dusza, J.; Csanádi, T.; Ahmad, M.I.M.; Mat, M.F.; Dogahe, K.J. Assessing Fatigue Life Cycles of Material X10CrMoVNb9-1 through a Combination of Experimental and Finite Element Analysis. *Metals* **2023**, *13*, 1947. [[CrossRef](#)]
9. MIL-STD-1530C; Department of Defense Standard Practice: Aircraft Structural Integrity Program (ASIP). U.S. Department of Defense: Washington, DC, USA, 2016.
10. Ritchie, R.O.; Liu, D. *Introduction to Fracture Mechanics*; Elsevier: Amsterdam, The Netherlands, 2021.
11. Berens, A.; Hovey, P.; Skinn, D. *Risk Analysis for Aging Aircraft Fleets-Volume 1: Analysis, WL-TR-91-3066*; Technical Report; Flight Dynamics Directorate, Wright Laboratory, Air Force Systems Command, Wright-Patterson Air Force Base: Dayton, OH, USA, 1991.
12. Main, B.; Molent, L.; Singh, R.; Barter, S. Fatigue crack growth lessons from thirty-five years of the Royal Australian Air Force F/A-18 A/B hornet aircraft structural integrity program. *Int. J. Fatigue* **2020**, *133*, 105426. [[CrossRef](#)]
13. White, P.; Molent, L.; Barter, S. Interpreting fatigue test results using a probabilistic fracture approach. *Int. J. Fatigue* **2005**, *27*, 752–767. [[CrossRef](#)]
14. Gallagher, J.; Molent, L. The equivalence of EPS and EIFS based on the same crack growth life data. *Int. J. Fatigue* **2015**, *80*, 162–170. [[CrossRef](#)]
15. Liang, Y.; Dávila, C.; Iarve, E. A reduced-input cohesive zone model with regularized extended finite element method for fatigue analysis of laminated composites in Abaqus. *Compos. Struct.* **2021**, *275*, 114494. [[CrossRef](#)]
16. Babuska, I.; Sawlan, Z.; Scavino, M.; Szabó, B.; Tempone, R. Bayesian inference and model comparison for metallic fatigue data. *Comput. Methods Appl. Mech. Eng.* **2016**, *304*, 171–196. [[CrossRef](#)]
17. Pascual, F.G.; Meeker, W.Q. Analysis of fatigue data with runouts based on a model with nonconstant standard deviation and a fatigue limit parameter. *J. Test. Eval.* **1997**, *25*, 292–301. [[CrossRef](#)]
18. Pascual, F.G.; Meeker, W.Q. Estimating fatigue curves with the random fatigue-limit model. *Technometrics* **1999**, *41*, 277–289. [[CrossRef](#)]
19. Ryan, K.J. Estimating expected information gains for experimental designs with application to the random fatigue-limit model. *J. Comput. Graph. Stat.* **2003**, *12*, 585–603. [[CrossRef](#)]
20. Schijve, J. A normal distribution or a Weibull distribution for fatigue lives. *Fatigue Fract. Eng. Mater. Struct.* **1993**, *16*, 851–859. [[CrossRef](#)]
21. Zou, Q.; Wen, J. Bayesian model averaging for probabilistic SN curves with probability distribution model form uncertainty. *Int. J. Fatigue* **2023**, *177*, 107955. [[CrossRef](#)]
22. Birnbaum, Z.; Saunders, S. A New Family of Life Distributions. *J. Appl. Probab.* **1969**, *6*, 319–327. [[CrossRef](#)]
23. Birnbaum, Z.W.; Saunders, S.C. Estimation for a family of life distributions with applications to fatigue. *J. Appl. Probab.* **1969**, *6*, 328–347. [[CrossRef](#)]
24. Engelhardt, M.; Bain, L.J.; Wright, F.T. Inferences on the Parameters of the Birnbaum–Saunders Fatigue life Distribution Based on Maximum likelihood Estimation. *Technometrics* **1981**, *23*, 251–256. [[CrossRef](#)]
25. Achcar, J.A. Inferences for the Birnbaum–Saunders fatigue life model using Bayesian methods. *Comput. Stat. Data Anal.* **1993**, *15*, 367–380. [[CrossRef](#)]
26. Tsonas, E.G. Bayesian inference in Birnbaum–Saunders regression. *Commun. Stat.-Theory Methods* **2001**, *30*, 179–193. [[CrossRef](#)]
27. Xu, A.; Tang, Y. Bayesian analysis of Birnbaum–Saunders distribution with partial information. *Comput. Stat. Data Anal.* **2011**, *55*, 2324–2333. [[CrossRef](#)]
28. Rieck, J.R.; Nedelman, J.R. A log-linear model for the Birnbaum–Saunders distribution. *Technometrics* **1991**, *33*, 51–60.
29. Kundu, D. Bivariate log Birnbaum–Saunders distribution. *Statistics* **2015**, *49*, 900–917. [[CrossRef](#)]
30. Leiva, V. *The Birnbaum–Saunders Distribution*; Academic Press: Cambridge, MA, USA, 2015.
31. Balakrishnan, N.; Kundu, D. Birnbaum–Saunders distribution: A review of models, analysis, and applications. *Appl. Stoch. Model. Bus. Ind.* **2019**, *35*, 4–49. [[CrossRef](#)]

32. Grover, H.J.; Bishop, S.M.; Jackson, L.R. *Fatigue Strengths of Aircraft Materials: Axial-Load Fatigue Tests on Unnotched Sheet Specimens of 24S-T3 and 75S-T6 Aluminum Alloys and of SAE 4130 Steel*; NACA TN 2324; National Advisory Committee on Aeronautics: Washington, DC, USA, 1951.
33. Hyler, W.S.; Lewis, R.A.; Grover, H.J. *Experimental Investigation of Notch-Size Effects on Rotating-Beam Fatigue Behavior of 75S-T6 Aluminum Alloys*; NACA TN 3291; National Advisory Committee on Aeronautics: Washington, DC, USA, 1954.
34. Shimokawa, T.; Hamaguchi, Y. Statistical evaluation of fatigue life and fatigue strength in circular-hole notched specimens of a carbon eight-harness-satin/epoxy laminate. In *Statistical Research on Fatigue and Fracture (A 88-51351 22-39)*; Elsevier Applied Science: London, UK; New York, NY, USA, 1987; pp. 159–176.
35. Akaike, H. Information Theory and An Extension of the Maximum Likelihood Principle. In *Breakthroughs in Statistics, Volume I*; Springer: Berlin/Heidelberg, Germany, 1992; pp. 610–624.
36. Schwarz, G. Estimating the dimension of a model. *Ann. Stat.* **1978**, *6*, 461–464. [[CrossRef](#)]
37. Neath, A.A.; Cavanaugh, J.E. The Bayesian information criterion: Background, derivation, and applications. *Wiley Interdiscip. Rev. Comput. Stat.* **2012**, *4*, 199–203. [[CrossRef](#)]
38. Burnham, K.P.; Anderson, D.R. *Model Selection and Multimodel Inference*, 2nd ed.; Springer: Berlin/Heidelberg, Germany, 2002.
39. Walker, K. The effect of stress ratio during crack propagation and fatigue for 2024-T3 and 7075-T6 aluminum. *Eff. Environ. Complex Load Hist. Fatigue Life* **1970**, *462*, 1–14.
40. Huang, X.; Moan, T. Improved modeling of the effect of R-ratio on crack growth rate. *Int. J. Fatigue* **2007**, *29*, 591–602. [[CrossRef](#)]
41. Babuška, I.; Sawlan, Z.; Scavino, M.; Szabó, B.; Tempone, R. Spatial Poisson processes for fatigue crack initiation. *Comput. Methods Appl. Mech. Eng.* **2019**, *345*, 454–475. [[CrossRef](#)]
42. Chen, J.; Liu, S.; Zhang, W.; Liu, Y. Uncertainty quantification of fatigue SN curves with sparse data using hierarchical Bayesian data augmentation. *Int. J. Fatigue* **2020**, *134*, 105511. [[CrossRef](#)]
43. Meeker, W.Q.; Escobar, L.A.; Pascual, F.G.; Hong, Y.; Liu, P.; Falk, W.M.; Ananthasayanam, B. Modern Statistical Models and Methods for Estimating Fatigue-Life and Fatigue-Strength Distributions from Experimental Data. *arXiv* **2022**, arXiv:2212.04550.
44. Li, Y.Z.; Zhu, S.P.; Liao, D.; Niu, X.P. Probabilistic modeling of fatigue crack growth and experimental verification. *Eng. Fail. Anal.* **2020**, *118*, 104862. [[CrossRef](#)]
45. Molent, L.; Wanhill, R. Management of airframe in-service pitting corrosion by decoupling fatigue and environment. *Corros. Mater. Degrad.* **2021**, *2*, 493–511. [[CrossRef](#)]
46. Zhang, Y.; Zheng, K.; Heng, J.; Zhu, J. Corrosion-fatigue evaluation of uncoated weathering steel bridges. *Appl. Sci.* **2019**, *9*, 3461. [[CrossRef](#)]

Disclaimer/Publisher’s Note: The statements, opinions and data contained in all publications are solely those of the individual author(s) and contributor(s) and not of MDPI and/or the editor(s). MDPI and/or the editor(s) disclaim responsibility for any injury to people or property resulting from any ideas, methods, instructions or products referred to in the content.